Use of ENSO Information in Medium- and Long-Range Forecasting of the Nile Floods

GUILING WANG AND ELFATIH A. B. ELTAHIR

Ralph M. Parsons Laboratory, Department of Civil and Environmental Engineering, Massachusetts Institute of Technology, Cambridge, Massachusetts

(Manuscript received 21 November 1997, in final form 15 April 1998)

ABSTRACT

The natural variability in the annual flow of the Nile is significantly regulated by the El Niño–Southern Oscillation (ENSO). In this paper, several sources of information are combined, including ENSO, rainfall over Ethiopia, and the recent history of river flow in the Nile, in order to obtain accurate forecasts of the Nile flood at Aswan. The Bayesian theorem is used in developing the discriminant forecasting algorithm. Conditional categoric probabilities are used to describe the flood forecasts, and a synoptic index is defined to measure the forecasts' skill. The results presented show that ENSO information is the only valuable predictor for the long-range forecasts (lead time longer than the hydrological response timescale, which is 2–3 months in this study). However, the incorporation of the rainfall and river flow information in addition to the ENSO information significantly improves the quality of the medium-range forecasts (lead time shorter than the hydrological response timescale).

1. Introduction

The Nile, running for 6690 km, is one of the longest rivers in the world. Three main tributaries, the Blue Nile, White Nile, and Atbara River, contribute 70%, 20%, and 10%, respectively, of total Nile discharge (Hurst 1957). Covering most of the northeastern quarter of Africa, the Nile basin has nurtured one of the most ancient human civilizations. The Nile's flow is the main source of water in Egypt. In the late nineteenth century, from 1860–80, four serious floods caused severe property damage and loss of life in the Nile basin (Hurst 1957). However, in the present century, the Nile basin area has been suffering from water deficits. To protect this region against droughts, as well as possible floods, the High Aswan Dam was constructed in the 1960s. The most important function of the reservoir at Aswan is to hold back water from the flood season for use in the low flow season, and from wet years to supplement the water supply in drought years. According to the historical record, the flood peak in the Nile often occurs in September (Fig. 1a). This causes the months June, July, and August to be a critical time for the reservoir operation. The fact that these months are also important irrigation time makes reservoir operations more complex. To make full use of the often limited water, and to operate the reservoir in an optimal way, a high quality medium- to long-range forecast of the Nile flood is necessary. In this paper, we use the term ''medium range'' to describe forecasts with a lead time comparable to the timescale of the hydrological response, and the term ''long range'' to describe forecasts with a lead time longer than the hydrological response timescale. Here, the hydrological response time is the time lag between the precipitation event over the Nile catchment and the runoff delivered to Aswan station, which is about 2–3 months. The lead time is defined relative to the time of flood peak at Aswan station, which usually occurs in September.

The El Niño–Southern Oscillation (ENSO) phenomenon plays an important role in the medium- to long-range forecasts that we will present in this study. Previous studies have shown that ENSO is correlated with the interannual variability of rainfall and river flow in several regions of the world. An early study by Bliss (1925) showed that Nile flow is correlated with the pressure fluctuations at Port Darwin in Australia, that is, the Southern Oscillation. The cross-spectral analysis by Richey et al. (1989) showed a significant coherency between Amazon River discharge and ENSO. According to this study, low flow in the Amazon River tends to take place following major El Niño events. Kahya and Dracup (1993, 1994) and Dracup and Kahya (1994) studied the influence of ENSO on the U.S. streamflow, and found that the river flow in the United States, especially in the north-central region and the Pacific Northwest, does respond to the El Niño–La Niña events. Piechota and Dracup (1996) concentrated on the

Corresponding author address: Ms. Guiling Wang, Ralph M. Parsons Laboratory, Dept. of Civil and Environmental Engineering, Massachusetts Institute of Technology, Cambridge, MA 02139.
E-mail: glwang@mit.edu

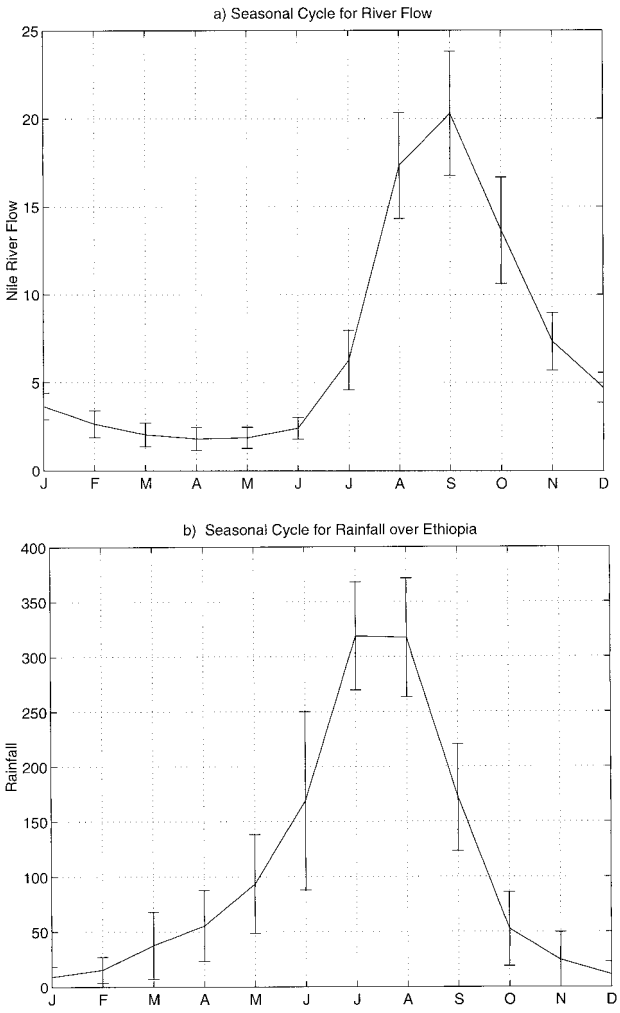

FIG. 1. The seasonal cycles for (a) Nile flow at Aswan and (b) rainfall over Ethiopia. Rainfall is measured in mm month^{-1}, and river flow is in km^3 month^{-1}.

droughts in the United States and found that El Niño has the strongest effect on extreme droughts in the Pacific Northwest. ENSO was also found to be correlated with rainfall and river flow in Australia by several previous studies (e.g., McBride and Nicholls 1983; Ropelewski and Halpert 1987, 1989). The study by Ropelewski and Halpert (1987, 1989) also showed that the Ethiopia Plateau is one of the several regions in the world where interannual fluctuations of rainfall are associated with ENSO. Camberlin (1995) confirmed this result by showing that drought conditions in Ethiopia are associated with El Niño events. The association between ENSO and the rainfall over Ethiopia contributes to the teleconnection between ENSO and Nile discharge, since the Blue Nile, which is the largest tributary of the Nile, drains the Ethiopian Plateau. According to Amarasekera et al.'s (1997) analysis, the correlation between ENSO and the discharge of the Nile is the most robust among four major tropical rivers: the Nile, Amazon, Congo, and Parana. This correlation is the basis of the proposed methodology for forecasting the Nile flood using the ENSO information.

Traditional river flow forecasting (e.g., Singh 1995) has a very short lead time, usually shorter than the hydrological response time. Since the 1980s, due to the successful ENSO predictions (Cane et al. 1986; Zebiak and Cane 1987) with a lead time of 1 yr or even longer, long-range river flow forecasting has been made possible using the ENSO–river flow teleconnection. When the predicted ENSO index is used as the river flow predictor, the forecasting lead time could be much longer than the hydrological response timescale. Simpson et al. (1993a,b) used ENSO to forecast the annual discharge of Australian rivers, with a lead time up to 1 yr. These studies brought a new perspective to the river flow forecasting. Similarly, Eltahir (1996) examined the significant correlation between ENSO and Nile discharge, and used ENSO as a predictor for his long-range forecasting for the Nile floods. In all these studies, ENSO is the only predictor for the river flow. To improve the forecast skill, additional information, if available, should be incorporated into the forecasting process. Precipitation over the drainage area of the river, river flows observed prior to the forecasting time, and any other relevant factor could be valuable sources of information for the river flow forecasting. The objective of this study is to develop a forecasting algorithm that could make use of several sources of information. Our predictand here is the annual flood of the Nile and the predictors include ENSO, rainfall over Ethiopia, and the prior streamflow of the Nile at Aswan.

For any forecasting problem, there are two frequently used forecasting approaches: the linear regression and the discriminant prediction. The regression approach, with single or multiple predictors, uses the best-fit relationship to estimate the predictand, while the discriminant approach estimates the probabilities that the predictand will fall into a set of prescribed categories. The statistical techniques of these two methods are described in Parsons (1978) and Afifi and Azen (1979). Which method to use usually depends on the particular prediction problem of interest. For purposes of operational decision-making, for example, reservoir operations, the most desirable information would be the full description of the uncertainties, that is, the probability distribution over the possible events for given values of the predictors. The operational decision can be made efficiently from a measure of the categorical probabilities (Miller 1962). In this study, we take the discriminant prediction approach, which has been frequently used in hydrological forecasts (Folland et al. 1991; Simpson et al. 1993a,b; Eltahir 1996).

In the next six sections, we will present our forecasting algorithm and its application in the annual flood forecasting for the Nile. The forecasting algorithm is based on the discriminant approach and is developed using the Bayesian theorem. As mentioned above, our

forecasts for the Nile flood combine the information from three sources: ENSO, rainfall over Ethiopia, and the prior streamflow of the Nile at Aswan. The data used in this study are described in section 2, followed by a spectral and cross-spectral analysis in section 3. Section 4 introduces the forecasting methodology. Section 5 details the application of the Bayesian theorem and the proposed algorithm. Section 6 presents the results, including calibration and verification of the algorithm. The conclusions are presented in section 7.

2. Data description

The data we use in this study include data on the Nile's flow, rainfall over the Ethiopian Plateau, and the ENSO index. The river flow data is the naturalized streamflow at Aswan, from January 1872 to December 1986. The seasonal cycle of the river flow data is shown in Fig. 1a. The river flow in May is the lowest of the whole year, and the flow peak occurs in September. Here we define 1 June as the beginning of a hydrological year and 31 May as the end. The annual Nile flood is defined as the accumulated river flow in each hydrological year. The rainfall data is taken from a global monthly rainfall dataset, gridded at a resolution of 3.75° lat × 2.5° long (Hulme 1995). This dataset covers the years from 1900 to 1994. We use the average in the region 7.5°–12.5°N, 37.5°–41.25°E over the Ethiopian Plateau, which covers most of the Blue Nile catchment. Figure 1b shows the rainfall seasonal cycle, with the maximum rainfall taking place in July. Comparison between Figs. 1a and 1b suggests that the hydrological response timescale is approximately 2–3 months. The ENSO index is derived from a monthly series of the sea surface temperature (SST) anomaly with respect to the SST climatology (Wright 1989). Following Eltahir (1996), we use the SST anomaly averaged over regions 6°–2°N, 170°–90°W; 2°N–6°S, 180°–90°W; and 6°–10°S, 150°–110°W as the monthly ENSO index. In forecasting the Nile floods, the ENSO index averaged from September through November is used because the correlation between the Nile annual discharge and the ENSO index during September–November is the highest compared with other seasons (Eltahir 1996, Table 1). The temporal coverage of the ENSO data is 1872–1986.

In the forecasting study, the ENSO index will be used as one of the Nile discharge predictors. For the purpose of forecasting, only the forecasts made before the flood peak (in September) are useful. However, the ENSO index we use is the SST anomaly from September to November for that same year and cannot be measured until after the flood peak. Therefore, the ENSO prediction is needed in order to make real-time forecasts. In section 6, a predicted ENSO index, provided by Dr. S. E. Zebiak of Lamont-Doherty Geological Observatory of Columbia University, for the period 1973–86, will be used to verify the efficiency of the ENSO prediction for the purpose of Nile flood forecasting. This predicted ENSO index is Zebiak and Cane's (1987) Nino-3 index with a lead time of 12 months.

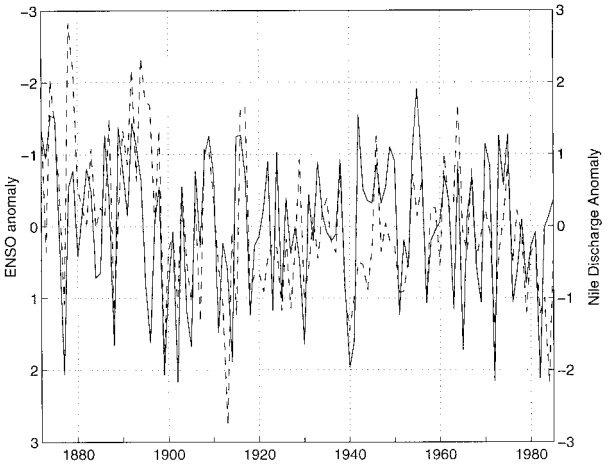

FIG. 2. Time series of the normalized anomalies of Sep–Nov ENSO index (solid line) and the annual Nile discharge (dash line). For the convenience of comparison, the two variables are plotted using opposite coordinates. The ''normalized anomalies'' stand for the anomalies divided by the standard deviation.

All the data used in the forecasting study are for the period 1900–85, which is the overlapping period for all the variables.

3. Spectral analysis

The use of rainfall and prior river flow in the annual flood forecasting has an explicit hydrological motivation. However, the use of ENSO in the Nile flood forecasting is based on the observed teleconnection between these two variables (Ropelewski and Halpert 1987; Camberlin 1995; Eltahir 1996). Figure 2 plots the normalized anomalies of the Nile annual discharge and that of the September–November ENSO index. For the convenience of comparison, these two time series are plotted in opposite coordinates. As shown in Fig. 2, in most of the major El Niño events, the Nile discharge is extremely low. The converse effect, high discharge associated with La Niña events, is also very obvious. The linear regression between the September–November ENSO index and the Nile annual discharge yields a correlation coefficient of -0.52. To confirm this correlation, here we conduct a spectral and cross-spectral analysis. Data used in this section are the monthly Nile flow and Wright's (1989) monthly ENSO index in their overlapping period 1872–1986.

The spectrum of Nile flow and that of ENSO are shown in Figs. 3a and 3b, respectively. Consistent with previous studies (e.g., Trenberth and Shea 1987), the power spectrum of ENSO is characterized by a broad peak that extends over 3–10-yr (40–120 month) periods. On the contrary, Nile flow has a distinguished peak at a period of about 1 yr (12 months), although the data used here has been deseasonalized by subtracting the

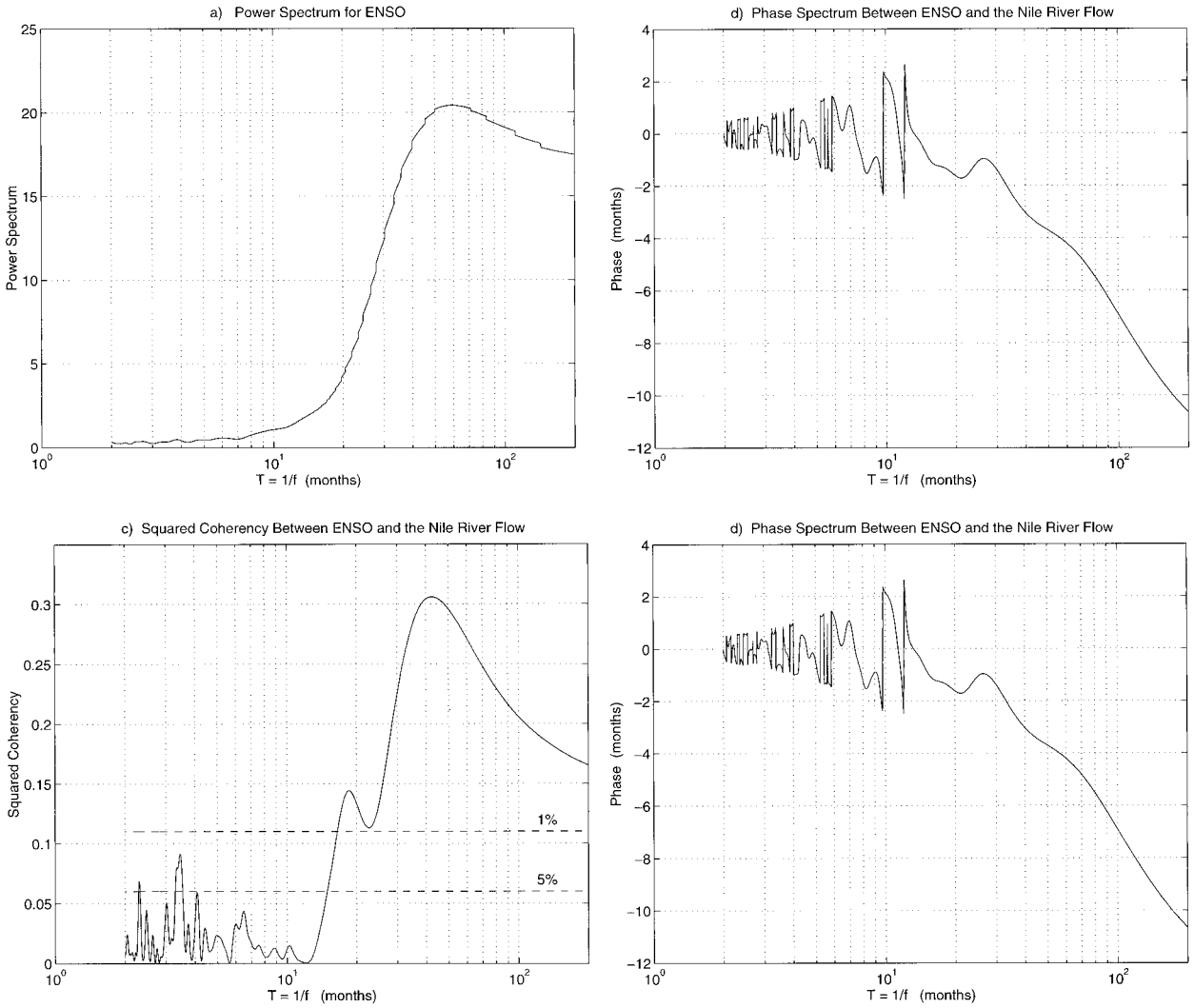

FIG. 3. (a) The power spectrum of ENSO, (b) the power spectrum of Nile flow, (c) the squared coherency, and (d) the phase spectrum between ENSO index and Nile flow. The monthly ENSO index and river flow data in the period 1872–1985 are used in these analyses. The two dashed lines in (c) show the 5% and 1% significance level, respectively.

means and dividing by the standard deviations for different calendar months. Besides that, the power spectrum of Nile flow at very long periods is also very high. Therefore, the seasonal variability and the long-term variability in Nile flow are dominant. Figures 3c and 3d show the squared coherency and the phase spectrum between ENSO and Nile flow. As shown in Fig. 3c, the coherence-square between Nile flow and ENSO exceeds the 1% significance level in most of the frequency domain, with a broad peak in the 3–6-yr (40–70-month) period range. This suggests that the variability of Nile flow, on the timescales of 3–6 yr, is significantly correlated with ENSO. The phase spectrum (Fig. 3d) at the corresponding timescale indicates that the anomaly of Nile flow lags the anomaly of the ENSO index by about 3–5 months. Therefore, the ENSO index carries valuable forecasting information about Nile flow.

Although the correlation between ENSO and the worldwide river flow has long been recognized, the physical mechanism involved remains a subject for active research. Our spectral analysis presents evidence of the association between the ENSO phenomena and Nile discharge. It does not shed light on the physical mechanism behind the teleconnection. According to the cross-spectral analysis, ENSO leads Nile flow by about 3–5 months. However, the correlation between the annual discharge and the seasonal ENSO index gets its maximum in the September–November season following the Nile flood peak (Eltahir 1996). This might be due to the fact that the ENSO signal is the strongest, therefore most detectable, in that season. As mentioned in section 2, the averaged ENSO index from September through November will be used as a predictor of the annual Nile discharge. Hereafter, when we talk about

TABLE 1. Coefficients of determination (R^2) between different variables. The variable ''flood'' is the annual Nile flood. The variable ''ENSO'' is the monthly ENSO index averaged from Sep through Nov. ''Rainfall'' stands for the accumulated rainfall amount from May to the different forecasting time (Jun, Jul, or Aug). ''River flow'' is the accumulated discharge from Jun to the forecasting time.

		Different time		
Variable 1	Variable 2	Jun	Jul	Aug
Flood	Rainfall	0.13	0.22	0.30
Flood	River flow	0.07	0.22	0.56
Flood	ENSO	0.27	0.27	0.27
ENSO	Rainfall	0.05	0.04	0.14
ENSO	River flow	0.00	0.09	0.12
Rainfall	River flow	0.00	0.05	0.21

predictors of the Nile floods, we will simply mention ''ENSO index'' without specifying that it is the September–November value.

4. Methodology

Nile flood forecasts can be made at any time of the year, although for the forecasting purpose only those forecasts made before the flood peak are useful. We perform our forecasts on the last day of each calendar month, from January to December. The forecasts after September are presented for comparison. For any forecast made before the beginning of the hydrological year, no rainfall or river flow information about that hydrological year is available, so we simply use the latest monthly rainfall and river flow observations available as the sources of information. For the forecasts made after 1 June, the total river flow from the beginning of June accumulated up to that time is used as one predictor. Due to the time lag between rainfall and river flow, rainfall in May of the last hydrological year also contributes to the annual flood of the current hydrological year, so the rainfall information used is the total rainfall accumulated since the beginning of May. The correlations of annual Nile flood with corresponding accumulated rainfall and river flow at different times are analyzed and tabulated in Table 1. The first two rows of Table 1 list the coefficients of determination between the annual flood and the amount of rainfall and river flow used in the forecasts on the last day of June, July, and August. As the time moves further into the hydrological year, the correlation coefficients become larger, therefore the rainfall and river flow information become more useful for the forecasting process. Obviously, when the forecasting time moves toward the end of the hydrological year, it is obvious that the coefficient of determination between the accumulated river flow and the annual flood will approach 1.0.

The discriminant prediction we use here is also called ''categoric prediction,'' which forecasts the categoric probabilities of the predictand according to the categories that the predictors fall into. All the data points are divided into three categories, as is done in many of the previous studies (Simpson et al. 1993a,b; Eltahir 1996). The data of Nile flow and annual flood are classified into ''low,'' ''normal,'' and ''high'' categories. The rainfall data categories are labeled ''dry,'' ''normal,'' and ''wet.'' Similarly, the ENSO index is categorized as ''cold,'' ''normal,'' and ''warm.'' For the Nile flood, rainfall, and prior river flow, the definition of normal is the range from $\mu - \sigma/2$ to $\mu + \sigma/2$ (μ is the mean value and σ is the standard deviation). The other two categories contain those data lower and higher than normal. For the ENSO index, we follow Simpson et al. (1993b) and Eltahir (1996) to use -0.5°C and 0.5°C as the boundaries for the ''normal'' category. Any condition with an ENSO index lower than -0.5° is defined as cold, and higher than 0.5°C, as warm. The way we define the boundaries between different categories is not totally arbitrary. It is designed in such a way that the number of data points contained in every category of a specific variable are not dramatically different from each other. In the real forecasts, the division of the categories, even the number of the categories, depends on the particular forecast purpose. For example, when only the extreme events (e.g., extremely wet or dry events, or the extreme El Niño or La Niña episodes) are considered, a much wider range for the ''normal'' category or a larger number of categories are recommended.

The categoric probabilities for the predictand, in this case the annual flood in the Nile river, will be the forecast results. For the forecasts that have three predictors, the categoric probability is the conditional probability with three conditions, that is, the probability of having a Nile flood in any category (low, normal, and high) given a certain category of ENSO condition (cold, normal, or warm), a certain category of rainfall condition (dry, normal, or wet), and a certain category of river flow condition (low, normal, or high). To compute these conditional probabilities, an algorithm is developed using the Bayesian theorem, as will be described in section 5. For a specific year, the forecasting results would be the three probabilities for the annual flood falling into each of its three categories. However, generally, the forecast is expressed by the forecasting probabilities of each category of the Nile flood given every possible combination of ENSO, rainfall, and river flow conditions. To easily judge the forecasts skill and to compare different forecasts, we propose a synoptic parameter, the forecasting index (FI), which can measure the forecast skill not only in this study but also in any other discriminant forecast. The FI value is defined as the average of the forecasting categoric probabilities for the categories that the observed Nile flood in each individual year falls into during an n-yr period. First of all, in each year j ($j = 1, \ldots, n$), the ENSO index, rainfall, and river flow data are categorized. Accordingly, the probability of each Nile flood category can be forecasted, and we denote it as the prior probability $P_r(i, j)$, $i = 1, 2, 3$. Then, the Nile flood observation in that year is

categorized, and the posterior probability $P_p(i, j)$ can be identified as [1, 0, 0] in a low flow year, [0, 1, 0] in a normal year, and [0, 0, 1] in a high flow year. FP(j), the forecasting probability of the Nile flood category, which describes the observed flood condition for that year, can be computed as

$$\mathrm{FP}(j) = \sum_{i=1}^{3} P_r(i, j)P_p(i, j).$$

The forecasting index, FI, is the average of these probabilities over a certain period:

$$\mathrm{FI} = \frac{1}{n}\sum_{j=1}^{n} \mathrm{FP}(j) = \frac{1}{n}\sum_{j=1}^{n}\sum_{i=1}^{3} P_r(i, j)P_p(i, j). \quad (1)$$

A larger forecasting index implies a more accurate forecast. A perfect forecasting methodology would have an FI of 1.0.

Traditionally, the discriminant forecast skill is measured using the proportion of correct forecasts, in which the right category of the predictand gets the highest predicted probability. Therefore, when the traditional skill measure is used, a forecast of 80% (wet), 15% (normal), and 5% (dry) for a wet year is no difference from a forecast of 40% (wet), 35% (normal), and 25% (dry). However, the skill measure proposed in this study can tell the ''accuracy'' difference between different forecasts, even if they might be all correct forecasts. This new measure of skill provides a better tool to judge the quality of categoric predictions.

5. The Bayesian theorem and forecasting algorithm

a. Algorithm development

Any conditional probability can be computed by counting all the relevant data points and normalizing it by the number of all data points that satisfy the condition or conditions. Here, we are interested in the conditional categoric probabilities. All the data points that fulfill the given condition(s) are counted; we then identify those cases with a low, normal, and high annual flood, and get the relative frequency distribution. Then the forecasting probability of each flood category can be computed. By counting the data points conditionally, the total data points are divided into several groups. If only one condition is considered, the relevant data points will be divided into nine groups, which is shown by Figs. 4a–c. To avoid statistical error, the number of the total data points should be much larger than the number of groups into which the whole record is divided by conditional counting. However, the number of groups increases exponentially with the number of conditions. Considering only two conditions results in 27 groups, and with three conditions we get 81 groups. Usually, the limited data size makes this process impractical.

In this study, we are dealing with the forecasting probability of the Nile flood using three sources of information (ENSO, rainfall, and prior river flow). Therefore, a conditional probability with three conditions is involved. To break through the limitation of data size, we develop an approximate algorithm using the Bayesian theorem. Details for Bayesian theory are described in many statistical books (e.g., Winkler 1972; West 1989).

The Bayesian theorem can be expressed as

$$P(Q_i/A, B) = \frac{P(B/Q_i, A)P(Q_i/A)}{P(B/A)}, \quad (2)$$

where $P(Q_i/A)$ is the possibility of event Q_i given that event A has occurred, and $P(Q_i/A, B)$ is the possibility of event Q_i given that both event A and event B have occurred. Here, $P(B/Q_i, A)$, $P(B/A)$, and the following probabilities can be defined in a similar manner. Assuming A and B are independent events, we can rewrite Eq. (2) as

$$P(Q_i/A, B) = \frac{P(B/Q_i)P(Q_i/A)}{\sum_{j=1}^{3} P(B/Q_j)P(Q_j/A)}, \quad (3)$$

where Q_j represents a full group of events. Equation (3) expresses $P(Q_i/A, B)$ as a function of $P(Q_i/A)$ and $P(B/Q_i)$, $i = 1, 2, 3$. When we compute $P(Q_i/A)$, $P(B/Q_i)$ by the counting procedure, we only need to divide the available data into nine groups. This can significantly reduce the statistical error resulting from a limited data size. The advantage of assuming independence in the Bayesian algorithm is that the records of the variables defining events A and B can be totally nonoverlapping. If we have the data on Q_i for both period 1 and period 2, and have data on A only in period 1 and data on B only in period 2, the conditional probability can still be computed using Eq. (3), because no relation between A and B is needed. This allows us to include more information beyond the overlapping period when the data in the overlapping period is too limited.

For the case including a third independent condition C, the conditional probability $P(Q_i/A, B, C)$ can be derived from Eq. (3).

Assume $D = A \cup B$; then C and D are independent since A, B, and C are independent. Therefore,

$$P(Q_i/D, C) = \frac{P(C/Q_i)P(Q_i/D)}{\sum_{j=1}^{3} P(C/Q_j)P(Q_j/D)}.$$

Substituting $D = A \cup B$ into the above equation yields

$$P(Q_i/A, B, C) = \frac{P(C/Q_i)P(Q_i/A, B)}{\sum_{j=1}^{3} P(C/Q_j)P(Q_j/A, B)}. \quad (4)$$

The conditional probability with more conditions can be derived similarly.

By substituting Eq. (3) into Eq. (4), a three-variable

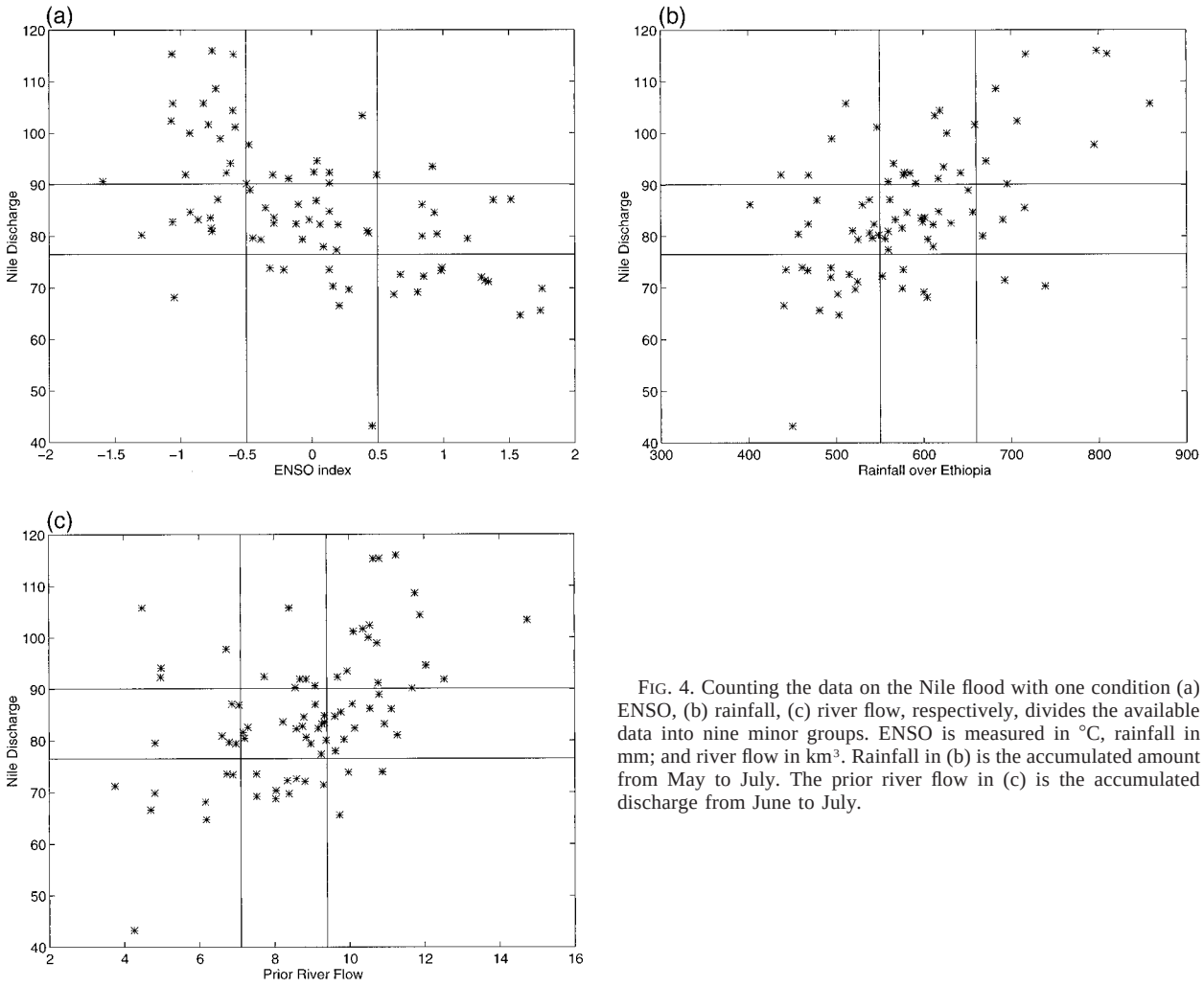

FIG. 4. Counting the data on the Nile flood with one condition (a) ENSO, (b) rainfall, (c) river flow, respectively, divides the available data into nine minor groups. ENSO is measured in °C, rainfall in mm; and river flow in km^3. Rainfall in (b) is the accumulated amount from May to July. The prior river flow in (c) is the accumulated discharge from June to July.

conditional probability can be computed from a set of one-variable conditional probabilities. If Q, E, P, and R stand for the Nile annual flood (Q), the ENSO (E) index, precipitation over Ethiopia (P), and prior Nile River flow (R), respectively, the forecasting probability $P(Q_i/E, P, R)$ is a function of $P(R/Q_j)$, $P(P/Q_j)$, $P(Q_j/E)$, $j = 1, 2, 3$.

To use Eqs. (3) and (4), we need to assume the independence between the input variables E, P, R. Although these three variables are correlated with one another, before September, the mutual correlation between them is relatively weaker than their correlations with the Nile annual flood, as shown in Table 1, which uses June, July, and August as examples. The upper half of the table lists the coefficients of determination between the annual Nile flood and each of the input variables; the lower half lists the coefficients of determination between each of the three input variables. In every month, the values in the lower half are much smaller than those in the upper half. Thus we can assume that the input variables are statistically independent, although physically they are not.

b. *Effect of the independence assumption*

To look at the influence of the assumption of independence between the predictors, a simple experiment is designed. The data we are using covers the period 1900–85. If only two predictors are considered, this record length is adequate for using the data-counting method to compute the conditional probability of the Nile flood. Here we forecast the Nile annual flood using any two of these three predictors (the ENSO index, rainfall, river flow) by applying both the Bayesian algorithm [Eq. (3)] and the data-counting procedure. As an example, Table 2 tabulates the results of the forecasts based on ENSO and rainfall information conducted in July. We list only the forecasting probabilities in the categories within which we have enough data points for the use of the data-counting procedure. For the other

TABLE 2. Nile flood forecast based on ENSO and rainfall information. The probabilities over the slash are derived using data counting, and those under the slash are the forecast results using the Bayesian algorithm.

Conditions		Flood		
ENSO	Rainfall	Low	Normal	High
Cold	Normal	0.14/0.02	0.64/0.66	0.21/0.32
	Wet	0.00/0.01	0.12/0.00	0.88/0.99
Normal	Dry	0.58/0.49	0.42/0.44	0.00/0.07
	Normal	0.33/0.19	0.61/0.73	0.06/0.08
Warm	Dry	0.77/0.79	0.23/0.19	0.00/0.02
	Normal	0.50/0.48	0.50/0.48	0.00/0.04

combinations of rainfall and ENSO categories, we have too few data points (less than 5 points) to conduct the counting procedure. In Table 2, the value over the ''/'' is derived in the data-counting procedure, and that under the ''/'' is derived using the Bayesian algorithm. As shown, there is very small difference in terms of the relative magnitude of the three probabilities; that is, the category that gets the highest probability in the data-counting process still has the highest probability when it comes to the Bayesian algorithm. The forecast skills measured by the FI values for the two methods are plotted in Fig. 5, which shows no systematic difference between these two. Figure 5 might imply that for the dataset size and correlation magnitude we are dealing with in this study, the statistical errors due to the data size limitation for the two-condition data-counting method has a similar magnitude as the errors caused by the independence assumption in the algorithm we developed in this study. In other words, the advantage brought to the forecasting process by breaking through the limitation of data size could compensate for the disadvantage caused by the approximate assumption. Comparison between the two methods for forecasts using other combinations of predictors (i.e., rainfall and river flow, or ENSO and river flow) supports the same conclusion. The benefit from Bayesian methodology is larger when we deal with three predictors. Therefore, in this study, the damage for the forecasts quality caused by the mutual dependence between ENSO index, rainfall over Ethiopia, and Nile flow could be small. Hence, we use Eqs. (3) and (4) in our study without considering the mutual dependence between the three predictors.

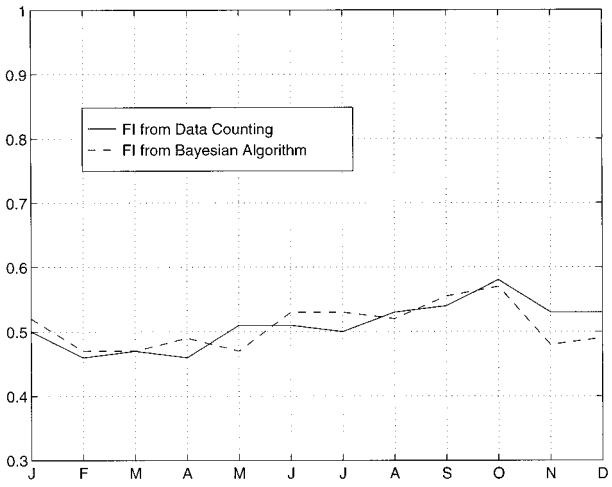

FIG. 5. The FI values for forecasts based on ENSO and rainfall information using two different methods: data counting and the Bayesian algorithm.

6. Results

Using the Bayesian algorithm developed in section 5, we forecast the Nile annual flood using information about ENSO, rainfall, and river flow as predictors. We conducted both a calibration and a verification analysis. The calibration period covers 50 yr, from 1900 to 1949, and the verification period is 36 yr-long, from 1950 to 1985.

Our main objective here is to forecast the Nile flood using three sources of information, the ENSO index, rainfall over Ethiopia, and prior Nile flow. To show the improvements that these three sources of information bring to the quality of the flood forecasting, the corresponding forecasts using two predictors, one predictor, and no predictor are also performed. The case with no predictor refers to a forecast based solely on the historical record of the annual flood, which is determined by the division of the annual discharge categories. In this case, using 1900–49 as the calibration period, the forecasting probabilities for the low, normal, and high flow categories are 30%, 44%, and 26%, respectively. The forecasts using the predictor(s) start by adding ENSO information, then adding the rainfall and river flow information. To show the importance of ENSO information, we also perform the forecasts using only rainfall and river flow as predictors. Although only the forecasts made before the Nile flood peak are useful, for comparison we also perform those after the time of the flood peak. For every case, the forecasting time extends from the end of January to the end of December. All the forecasts are made at the end of every month. To be compact, hereafter, we will only mention the name of that month when referring to the forecasts made at the end of the month.

Here we use July as an example to show the calibrated forecasting probabilities with three predictors, as tabulated in Table 3. Once the ENSO, rainfall, and prior river flow information for the July forecasts are collected, Table 3 will give the forecast probabilities. Suppose that in a specific year, the ENSO index is categorized as cold, and rainfall and river flow as wet and high, then the probabilities for the annual discharge to fall into the low, normal, and high categories are 1%, 10%, and 89%, respectively. In Table 3, it is worth noticing that the probability of having a high Nile flood is always zero when the ENSO index is in warm category, which means that no high flood has ever been

TABLE 3. The Nile flood probabilities for July forecast using ENSO, rainfall, and river flow information.

Predictors			Predictand (annual flood)		
ENSO	Rainfall	River flow	Low	Normal	High
Cold	Dry	Low	0.33	0.44	0.23
		Normal	0.25	0.65	0.10
		High	0.10	0.48	0.42
	Normal	Low	0.05	0.45	0.50
		Normal	0.04	0.72	0.24
		High	0.01	0.34	0.65
	Wet	Low	0.04	0.16	0.80
		Normal	0.05	0.37	0.58
		High	0.01	0.10	0.89
Normal	Dry	Low	0.66	0.29	0.05
		Normal	0.53	0.45	0.02
		High	0.34	0.52	0.14
	Normal	Low	0.21	0.59	0.20
		Normal	0.14	0.80	0.06
		High	0.06	0.59	0.35
	Wet	Low	0.47	0.29	0.24
		Normal	0.23	0.52	0.25
		High	0.06	0.25	0.69
Warm	Dry	Low	0.89	0.11	0.00
		Normal	0.82	0.18	0.00
		High	0.72	0.28	0.00
	Normal	Low	0.59	0.41	0.00
		Normal	0.42	0.58	0.00
		High	0.29	0.71	0.00
	Wet	Low	0.77	0.23	0.00
		Normal	0.63	0.37	0.00
		High	0.49	0.51	0.00

observed during major El Niño events in our calibration period. In Table 4, the forecasting probability for two extreme cases from Table 3 are compared with the forecasting results obtained by using the historical record and by using ENSO solely. It shows that the addition of ENSO information to the information from the historical record modifies the forecasting probability for the Nile flood to a large extent. Significant modification is also obtained by introducing the rainfall and prior river flow information in addition to ENSO. In both cases, the incorporation of additional information tends to result in a more definite forecast; that is, one of the three categoric probabilities stands out and the other two shrink.

Figures 6a and 6b demonstrate the skill measurements (FI values) of the different forecasts. As we explained in section 4, the FI value is computed by comparing the forecasts with the observations.

a. Calibration (1900–49)

Figure 6a shows the FI values for different forecasts in the calibration period. Based on the historical flood record, we obtain an FI value of about 0.35. Because the Nile flood data are divided into three categories, any FI value not significantly higher than one-third indicates a trivial forecast. The ENSO information introduces a

TABLE 4. Probabilities of the Nile flood in several extreme cases of the Jul forecasts. Type 1 stands for the forecasts based on the historical record; type 2 stands for the forecasts using ENSO as the predictor; type 3 stands for the forecasts using ENSO, rainfall, and river flow as predictors.

Predictors			Forecast type	Predictand (annual flood)		
ENSO	Rainfall	River flow		Low	Normal	High
Cold	Wet	High	1	0.30	0.44	0.26
			2	0.07	0.40	0.53
			3	0.01	0.10	0.89
Warm	Dry	Low	1	0.30	0.44	0.26
			2	0.67	0.33	0.00
			3	0.89	0.11	0.00

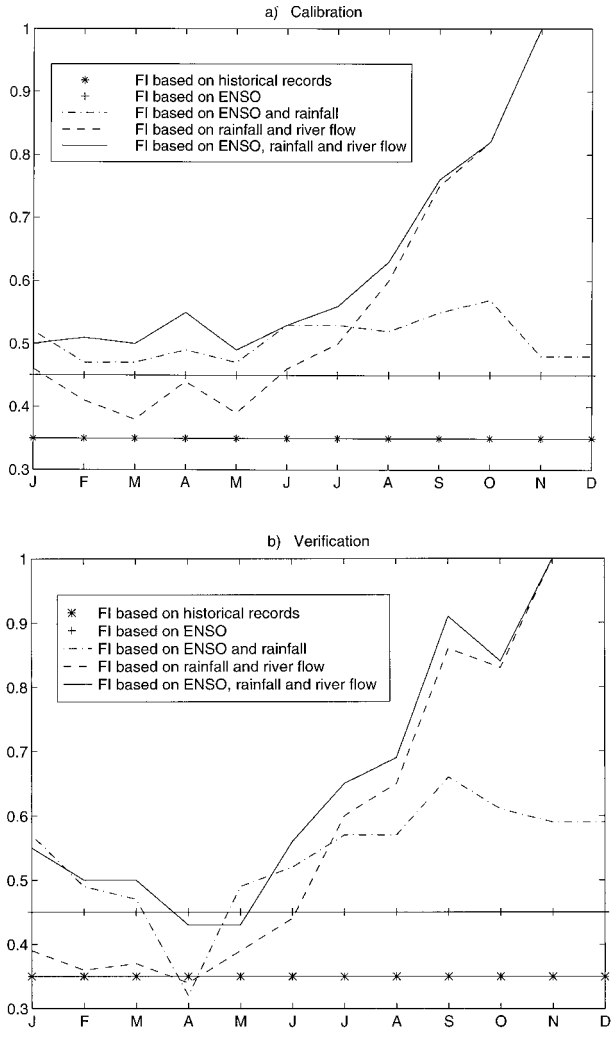

FIG. 6. The FI values in (a) calibration period (1900–49) and (b) verification period (1950–85).

significant improvement, with a jump of FI value as high as 0.1, from 0.35 to 0.45. It is worth noting that the skill improvement resulting from ENSO information does not change with the forecasting time: FI is as high as 0.45 (solid line with ''+'' sign) even as early as January. If the rainfall and river flow information are used in addition to the ENSO information, we get a forecasting index that changes with the forecasting time. Before June, which is the beginning of the hydrological year, the addition of rainfall and river flow information improves the forecasts skill by about 0.05. Skill comparison between the forecasts using all three predictors (solid line) and the forecasts using ENSO and rainfall (dash–dot line) shows that both the rainfall and river flow information contribute to this improvement. The dashed line in Fig. 6a represents the skill for the forecasts based on rainfall and river flow information. Before May, using rainfall or river flow as predictors is equivalent to assuming pure hydrological persistence. As shown, the forecast skills based on persistence (dash line) are much lower than those based on ENSO index (solid line with ''+'' sign). All these imply that for long-range forecasting, ENSO is the most important source of information. The rainfall and river flow information available before June are from the last hydrological year, so their role in the long-range forecasting of the flood in the current hydrological year is not as important as ENSO.

Since June, with more information about rainfall and river flow becoming available, the forecasting quality gains a larger improvement from the addition of rainfall and river flow information. The rainfall information boosts the FI value from 0.45 (solid line with ''+'' sign) to 0.53 (dash–dot line), which does not change significantly in the forecasts made from June to September. River flow information introduces additional improvement to the forecasting quality, which becomes higher and higher as the forecasting time progresses into the current hydrological year. These lead to an FI value for the forecasts using three predictors (solid line) as high as 0.56 in July and 0.63 in August. Notice that the Nile flow peak occurs in September. So on average, 2 months before the flood peak, we forecast a probability of 56% for the correct flood category, and 1 month before the flood peak, this forecasted probability is 63%. Comparing with the FI value for forecasts using ENSO information solely (0.45), we conclude that the rainfall and river flow information are very important in improving the forecasting quality of the medium-range forecasts. ENSO is also an important factor in the medium-range forecasting since there is still a big gap between the skills for forecasts using rainfall and river flow information and the skills for forecasts using ENSO, rainfall, and river flow information.

After the time of the flood peak, significant information about the river flow is available, thus it becomes almost trivial to identify the right category of the annual flood. As expected, the forecasting index approaches 1.0 when the river flow information is added to the forecasts.

b. Verification (1950–85)

The forecast skills in the verification period are shown in Fig. 6b. Similar to the results in the calibration period, ENSO is the most important information source for the long-range forecasts, and rainfall and river flow information improve the medium-range forecast skill. Two noticeable differences between the calibration and verification periods are observed:

1) In the verification period, there is a dip in the skill of April and May forecasts. This is caused by some change in the rainfall seasonal pattern over the Ethiopian Plateau. During the verification period, there are several extremely dry springs, with rainfall amount less than 20% of its normal value, followed by a very wet or normal summer. This kind of rainfall pattern, or the other way around (wet spring followed by dry summer), was not observed in the calibration period. This change of precipitation persistence causes the low forecast skill in April and May of the verification period.
2) The medium-range forecast skills in the verification period are generally higher than those in the calibration period. The FI value for forecasts using three predictors is 0.65 in July and 0.69 in August, compared with 0.56 and 0.63 in the calibration period. The FI value for the forecasts using ENSO solely is the same as in the calibration period. Therefore, rainfall and river flow bring more information to the medium-range forecasting in the verification period than in the calibration period.

As cited before, an FI not larger than 0.34 indicates a trivial forecast because the Nile flood is divided into three categories. It is worth noting that, because of the same reason, an FI value equal to or larger than 0.5 indicates a successful forecast. For example, suppose that in a wet year, the forecast probabilities for the three Nile flood categories are A (wet), B (normal), and C (dry), where $A + B + C = 1.0$. If $A > 0.5$, both B and C must be less than A. Therefore, a correct forecast is guaranteed regardless the values of B and C. For our forecasts with three predictors, the FI values are almost always larger than 0.5 in both the calibration and the verification periods.

c. Effect of ENSO prediction

In the above ''forecasts,'' the ENSO index is based on observation. However, in practice, we need to use the predicted ENSO index [SST anomaly in the tropical eastern Pacific Ocean (TEP) from September to November]. To investigate the influence of ENSO prediction on Nile flood forecasting, we compare the forecasts based on the ENSO prediction (''Pre.'' forecasts) with

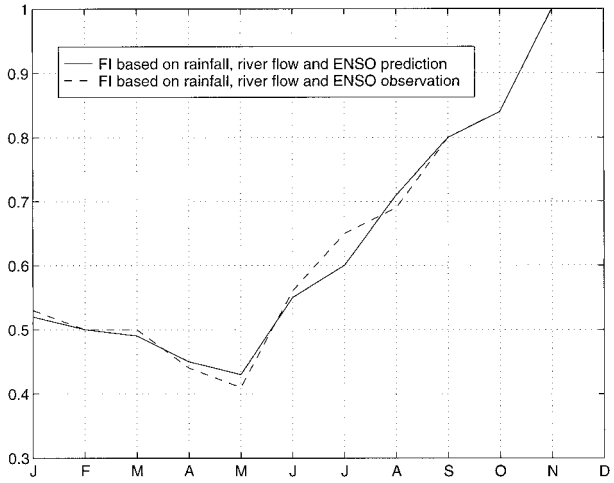

FIG. 7. FI value in a verification period 1973–86 for forecasts with three predictors using predicted ENSO index (solid line) and observed ENSO index (dashed line). The predicted ENSO index is Zebiak and Cane's (1987) Nino-3 index; the observed ENSO index was derived from Wright's SST data.

the hindcasts based on the ENSO observation (''Obs.'' forecasts). The predicted ENSO index covers the period 1973–85. Figure 7 plots the FI values for the forecasts with three predictors, using 1973–85 as the verification period. The dashed line stands for the Obs. forecasts, and the solid line stands for the Pre. forecasts. Similar to Fig. 6b, the low forecast skills in April and May are caused by the shift of the rainfall seasonal pattern. Figure 7 shows no significant difference in the FI value for the forecasts using ENSO prediction and ENSO observation, which suggests that the predicted ENSO index works as well as the observed one. The long-range forecasting of the Nile flood can rely on the predicted ENSO information.

7. Conclusions

The correlation between ENSO and the Nile discharge is the basis of the proposed methodology for the medium- to long-range forecasting of the Nile flood. The ENSO index solely yields a reasonably accurate forecast for the Nile flood, with an FI value of 0.45, compared to 0.35 for the forecast based solely on the historical record. In this study, we developed an algorithm to combine other information with ENSO, and performed medium- to long-range forecasting of the Nile flood using information about ENSO, rainfall over Ethiopia, and prior river flow of the Nile. For the long-range forecasting of the Nile flood (lead time longer than the hydrological response timescale), ENSO information plays the dominant role. However, for the medium-range forecasts (lead time shorter than the hydrological response timescale), information about rainfall and prior river flow brings large improvement to the forecasting quality. In June, July, and August, the FI values for the forecasts using three predictors are about 0.10–0.20 higher than the FI value for the forecasts using ENSO solely. By using these additional information sources, we achieved a significantly better medium-range forecast.

As discussed in section 6, an FI value larger than 0.5 implies a successful forecast since the forecast probability for the correct category is the highest of the three. The skill increase caused by the rainfall and river flow information, ranging from 0.05 to 0.20 in this study, boosted the FI value over 0.50 in almost all the forecasts using three predictors. Therefore, we view the improvement due to rainfall and river flow information as significant. Our medium- to long-range forecasts for the Nile river annual flood are successful.

For practical purposes, the predicted SST in TEP should be used as the ENSO index. Based on the results of this study, the ENSO prediction is good enough to be used in the medium- to long-range forecasting of the Nile flood. This assures the practicality of the forecasting procedure proposed in this paper.

Acknowledgments. We thank Dr. Stephen E. Zebiak for providing the SST predictions for the Pacific Ocean. Julie Kiang deserves credit for reviewing the manuscript. We also thank the anonymous reviewers for their helpful comments.

REFERENCES

Afifi, A. A., and S. P. Azen, 1979: *Statistical Analysis—A Computer Oriented Approach.* Academic Press, 442 pp.

Amarasekera, N. A., R. F. Lee, E. R. Williams, and E. A. B. Eltahir, 1997: ENSO and the natural variability in the flow of tropical rivers. *J. Hydrol.,* **200,** 24–39.

Bliss, E. W., 1925: Nile flood and world weather. *Mem. Roy. Meteor. Soc.,* **4,** 53–84.

Camberlin, P., 1995: June–September rainfall in north-eastern Africa and atmospheric signals over the tropics: A zonal perspective. *Int. J. Climatol.,* **15,** 773–783.

Cane, M. A., S. E. Zebiak, and S. C. Dolan, 1986: Experimental forecasts of El Niño. *Nature,* **321,** 827–832.

Dracup, J. A., and E. Kahya, 1994: The relationship between U.S. streamflow and La Nina events. *Water Resour. Res.,* **30,** 2133–2141.

Eltahir, E. A. B., 1996: El Niño and the natural variability in the flow of the Nile river. *Water Resour. Res.,* **32,** 131–137.

Folland, C., J. Owen, M. N. Ward, and A. Colman, 1991: Prediction of seasonal rainfall in the Sahel region using empirical and dynamical methods. *J. Forecasting,* **10,** 21–56.

Hulme, M., 1995: Estimating global changes in precipitation. *Weather,* **50,** 34–42.

Hurst, H. E., 1957: *The Nile, A General Account of the River and the Utilization of Its Water.* Constable, 326 pp.

Kahya, E., and J. A. Dracup, 1993: U.S. streamflow patterns in relation to the El Nino/Southern Oscillation. *Water Resour. Res.,* **29,** 2491–2503.

——, and ——, 1994: The influence type 1 El Niño and La Niña events on streamflows in the Pacific southwest of the United States. *J. Climate,* **7,** 965–976.

McBride, J. L., and N. Nicholls, 1983: Seasonal relationship between Australian rainfall and the Southern Oscillation. *Mon. Wea. Rev.,* **111,** 1998–2004.

Miller, R. G., 1962: *Statistical Prediction by Discriminant Analysis. Meteor. Monogr.*, No. 25, Amer. Meteor. Soc., 54 pp.

Parsons, R., 1978: *Statistical Analysis: A Decision-Making Approach.* Harper and Row, 791 pp.

Piechota, T. C., and J. A. Dracup, 1996: Drought and regional hydrologic variation in the United States: Association with the El Nino–Southern Oscillation. *Water Resour. Res.*, **32,** 1359–1373.

Richey, J., C. Nobre, and C. Deser, 1989: Amazon River discharge and climate variability: 1903 to 1985. *Science*, **246,** 101–103.

Ropelewski, C. F., and M. S. Halpert, 1987: Global and regional scale precipitation patterns associated with the El Niño/Southern Oscillation. *Mon. Wea. Rev.*, **115,** 1606–1626.

——, and ——, 1989: Precipitation patterns associated with the high-index phase of the Southern Oscillation. *J. Climate*, **2,** 268–284.

Simpson, H. J., M. A. Cane, A. L. Herczeg, S. E. Zebiak, and J. H. Simpson, 1993a: Annual river discharge in Southern Australia related to El Nino–Southern Oscillation forecasts of sea surface temperature. *Water Resour. Res.*, **29,** 3671–3680.

——, ——, S. K. Lin, A. L. Herczeg, and S. E. Zebiak, 1993b: Forecasting annual discharge of River Murray, Australia, from a geophysical model of ENSO. *J. Climate*, **6,** 386–390.

Singh, V. P., 1995: *Computer Models of Watershed Hydrology*. Water Resources Publications, 1130 pp.

Trenberth, K. E., and D. J. Shea, 1987: On the evolution of the Southern Oscillation. *Mon. Wea. Rev.*, **115,** 3078–3096.

West, M., 1989: *Bayesian Forecasting and Dynamic Models.* Springer, 704 pp.

Winkler, R., 1972: *An Introduction to Bayesian Inference and Decision.* Holt, Rinehart and Winston, 563 pp.

Wright, P. B., 1989: Homogenized long-period Southern Oscillation indices. *Int. J. Climatol.*, **9,** 33–54.

Zebiak, S. E., and M. A. Cane, 1987: A model El Niño–Southern Oscillation. *Mon. Wea. Rev.*, **115,** 2262–2278.